Influences of surface effects and large deformation on the resonant properties of ultrathin silicon nanocantilevers*

Zhang Jia-Hong(张加宏)[a)†], Li Min(李 敏)[a)], Gu Fang(顾 芳)[b)], and Liu Qing-Quan(刘清惓)[a)]

[a)] *Jiangsu Key Laboratory of Meteorological Observation and Information Processing, Nanjing University of Information Science & Technology, Nanjing* 210044, *China*

[b)] *College of Math & Physics, Nanjing University of Information Science & Technology, Nanjing* 210044, *China*

(Received 10 August 2011; revised manuscript received 14 October 2011)

The purpose of the present work is to quantify the influences of the discrete nature, the surface effects, and the large deformation on the bending resonant properties of long and ultrathin ⟨100⟩ silicon nanocantilevers. We accomplish this by using an analytical semi-continuum Keating model within the framework of nonlinear, finite deformation kinematics. The semi-continuum model shows that the elastic behaviors of the silicon nanocantilevers are size-dependent and surface-dependent, which agrees well with the molecular dynamics results. It also indicates that the dominant effect on the fundamental resonant frequency shift of the silicon nanocantilever is adsorption-induced surface stress, followed by the discrete nature and surface reconstruction, whereas surface relaxation has the least effect. In particular, it is found that a large deformation tends to increase the nonlinear fundamental frequency of the silicon nanocantilever, depending not only on its size but also on the surface effects. Finally, the resonant frequency shifts due to the adsorption-induced surface stress predicted by the current model are quantitatively compared with those obtained from the experimental measurement and the other existing approach. It is noticed that the length-to-thickness ratio is the key parameter that correlates the deviations in the resonant frequencies predicted from the current model and the empirical formula.

Keywords: resonant properties, elastic properties, surface effects, silicon nanocantilevers

PACS: 62.25.–g, 62.40.+i, 68.35.B–, 61.46.Km **DOI:** 10.1088/1674-1056/21/1/016203

1. Introduction

The strong demands for miniaturization in the field of nanoelectromechanical systems (NEMS)[1] have stimulated considerable efforts to fabricate and use nanoscale materials and structures as the fundamental building blocks for ultra-sensitive and ultrafine resolution applications. Silicon is the most remarkable semiconductor material. Consequently, silicon nanostructures, such as silicon nanocantilevers (SiNCs) and silicon nanowires (SiNWs), are attracting more and more interest due to their unique physical properties.[2−8] Specifically, Li *et al.*[2] have successfully measured the Young's modulus of SiNCs by using resonance experiments, while Kizuka *et al.*[3] have measured the atomistic mechanics of SiNWs by using tensile experiments. Those experiments revealed that the mechanical properties of silicon nanostructures were size- and surface-dependent. Cui *et al.*[4] experimentally examined the surface-dependent electrical performance of a SiNW field effect transistor (FET), and found that thermal annealing and surface passivation improved significantly the SiNW FET performance, i.e., the average transconductance and the average mobility were increased. Using a microfabricated suspended device, Li *et al.*[5] observed a strong size dependence of the thermal conductivity in SiNWs, which was more than two orders of magnitude lower than the bulk value. Recently, Wu *et al.*[6] investigated the mechanism and the enhancement of the photoluminescence from silicon nanocrystals, and found that the quantization effect, the interface states,

*Project supported by the National Natural Science Foundation of China (Grant No. 41075026), the Open Research Fund of Key Laboratory of MEMS of Ministry of Education, Southeast University, China (Grant Nos. 2009-03 and 2010-02), the Special Fund for Meteorology Research in the Public Interest, China (Grant No. GYHY200906037), and the Priority Academic Program Development of Sensor Networks and Modern Meteorological Equipment of Jiangsu Higher Education Institutions, China.

†Corresponding author. E-mail: zjhnuist@yahoo.cn

© 2012 Chinese Physical Society and IOP Publishing Ltd

and dangling bonds played important roles in the photoluminescence emission process. In addition, a theoretical study by Zhang *et al.*[7] showed that p-type SiNCs had enhanced electromechanical properties due to the quantization effect. Most strikingly, Yang and Li[8] have experimentally demonstrated that interface electron trapping could induce a giant piezoresistance in SiNCs, and compared to the conventional piezoresistance for bulk silicon, at least one order of magnitude higher piezoresistive coefficients were found in the p-type SiNCs.

In view of the remarkable mechanical, electrical, thermal, optical, and electromechanical properties of silicon nanostructures shown in Refs. [2]–[8], SiNCs have recently been proposed for a wide range of NEMS device applications, including force and pressure sensors, chemical and biological sensors, high frequency resonators, and many others.[9−11] Because many of the proposed applications, such as high frequency oscillators and resonant mass sensing, require precise knowledge about the resonant frequencies of SiNCs or the variations in the resonant frequencies due to environmental changes that are to be measured, it is critical to be able to predict, control, and tailor the resonant frequencies of SiNCs. However, the understanding and the design of such a SiNC-based NEMS are significantly complicated by the fact that the elastic properties and thus the resonant properties of SiNCs are known to differ from their macroscopic counterparts.

Due to the very small size and thus the large surface area to volume ratio of nanoscale structures, non-bulk mechanical responses are generally attributed to surface effects, including surface reconstruction (SREC), surface relaxation (SREL), surface stress (SSTR), surface energy, etc.[12−15] Therefore, understanding and modeling the non-bulk size-dependent mechanical properties of SiNCs due to surface effects is currently of particular interest. In the literature, various enhanced continuum models, molecular dynamics, and atomistic simulations have been employed to study the influence of surface effects on the size-dependent elastic properties of SiNCs.[12,13,16−21] However, we have a minimal understanding of how the surface effects influence the resonance frequencies of SiNCs, and previous limited studies mainly focused on exploring the impact of the SSTR on the resonant characteristics of silicon nanostructures.[18,22−24] For example, Park studied the influence of the residual (strain-independent) and the surface elastic (strain-dependent) parts of the SSTR on the resonant properties of SiNWs by using the surface Cauchy–Born model.[22,23] Feng *et al.*[24] investigated the influence of the SSTR on the resonant frequencies of SiNWs using a three-dimensional (3D) finite element model. In order to capture the influences of other surface effects, such as the SREC, the SREL, and the adsorption-induced SSTR,[25] and to understand the size-dependent resonance behavior of SiNCs thoroughly, more research work should be done.

Recently, the present authors proposed an analytical semi-continuum Keating (SCK) model to investigate the influence of surface effects on the size-dependent elastic properties of silicon nanobeams and SiNWs.[13,26] The SCK model can give a reliable prediction of their mechanical behavior. Therefore, in this paper, we try to explicitly address the non-bulk elastic behavior and thus the resonant properties of SiNCs by developing that SCK model. On one hand, all of the SREC, the SREL, and the adsorption-induced SSTR are taken into consideration in the present SCK model. On the other hand, the present SCK model is derived within the framework of nonlinear finite deformation kinematics. Therefore, the impact of the deformed maximum deflection on the non-bulk resonant properties of SiNCs is also a focus of the study.

2. Theoretical model

2.1. SCK model for Young's modulus and Poisson's ratio of SiNC in simple tension state

In the present SCK model, the prototype of study is a fixed-free ⟨001⟩ ultrathin SiNC with both the SREC and the SREL, whose side view and cross-sectional schematics are shown in Fig. 1. The adsorption-induced SSTR dominates the surface deformation when the SiNC is bent. A rectangular coordinate system is used with x, y, and z axes along the length, the width, and the thickness directions, respectively. Along the z axis, the typical silicon crystal cell with lattice constant $4a = 5.43$ Å in the bulk is assumed to be one cell layer, while a relaxed silicon crystal cell with lattice constant $4ka = 5.43k$ Å in the surface layers is assumed to be one cell layer, where the average SREL coefficient k is introduced. According to the experiment and the theory results in Ref. [27], the equivalent value of k in silicon is about

0.9775–0.9925. However, for ultrathin nanostructures, the relaxation may be contractive ($k < 1$) or expansive ($k > 1$).[13,14,21] As shown in Fig. 1(b), the SiNCs are assumed to have $2N$ ($N = 1, 2, 3, \ldots$) typical unrelaxed cell layers and $2n$ ($n = 1, 2, 3, \ldots$) relaxed cell layers along the thickness direction.

In a crystal cell, the position of the atom that occupies the i-th, j-th rows, and l-th column can be identified by a unique expression (x_i, y_j, z_l), which will be simplified as (i, j, l). Due to the SREL and the (2×1) SREC,[13,17] the positions of the surface atoms are different from the ideal positions, as shown in Fig. 1(b). In particular, the top and the bottom surfaces are nonequivalent, as the atom bond chain and the (2×1) dimmer bonds exist along different directions. Thus, the bulk strain energy U_{ijl}^{Bulk} of the typical silicon crystal cell at (i, j, l),[26,28] the surface strain energy U_{ijl}^{SREL} of the relaxed silicon crystal cell at (i, j, l),[13] and the surface strain energy $U_{ijl}^{\mathrm{T-SREC-SREL}}$ ($U_{ijl}^{\mathrm{B-SREC-SREL}}$) of the upper part (the low part) of the top surface (the bottom surface) reconstructed and relaxed crystal cell at (i, j, l) are different and must be expressed respectively. Based on the anharmonic Keating model,[29] here we give the most complex strain energy of the (2×1) surface reconstructed and relaxed top surface cell at (i, j, l) in terms of components (ε_x, ε_y, ε_z, γ_{xy}, γ_{xz}, γ_{yz}) of the elastic strains and components (u''', v''', w''') of the internal strain,

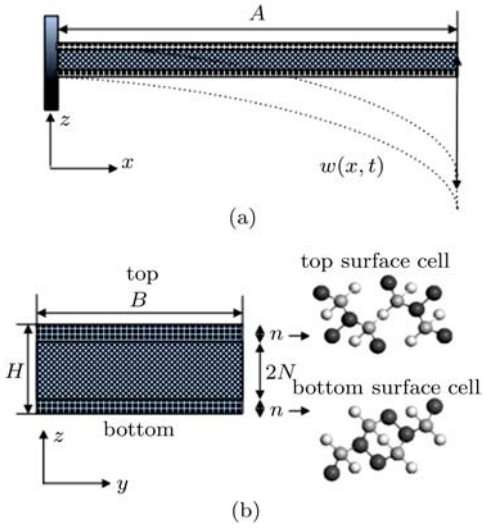


Fig. 1. (a) Side and (b) cross-sectional views of a SiNC with SREC, SREL, and adsorption-induced SSTR. The side view shows both undeformed and deformed SiNCs. The darker spheres represent atoms closer to the surfaces.

$$
\begin{aligned}
&U_{ijl}^{\mathrm{T-SREC-SREL}} \\
&= 2k_{\mathrm{b}}\{(2a-2\delta)^4(\varepsilon_x+\varepsilon_y+\gamma_{xy})^2 \\
&\quad + [(a+\delta)^2\varepsilon_x + (\delta-a)^2\varepsilon_y + k^2a^2\varepsilon_z + (\delta^2-a^2)\gamma_{xy} \\
&\quad - ka(a+\delta)\gamma_{xz} + ka(a-\delta)\gamma_{yz} + (a+\delta)u''' + (\delta-a)v''' - kaw''']^2 \\
&\quad + [(\delta-a)^2\varepsilon_x + (a+\delta)^2\varepsilon_y + k^2a^2\varepsilon_z + (\delta^2-a^2)\gamma_{xy} \\
&\quad + ka(a-\delta)\gamma_{xz} - ka(a+\delta)\gamma_{yz} + (\delta-a)u''' + (a+\delta)v''' - kaw''']^2 \\
&\quad + 2a^2(a\varepsilon_x + a\varepsilon_y + k^2a\varepsilon_z + a\gamma_{xy} + ka\gamma_{xz} + ka\gamma_{yz} + u''' + v''' + kw''')^2 \\
&\quad + 2a^2(a\varepsilon_x + a\varepsilon_y + k^2a\varepsilon_z + a\gamma_{xy} - ka\gamma_{xz} - ka\gamma_{yz} - u''' - v''' + kw''')^2 \\
&\quad + [(a-\delta)^2\varepsilon_x + (a+\delta)^2\varepsilon_y + k^2a^2\varepsilon_z + (\delta^2-a^2)\gamma_{xy} \\
&\quad - ka(a-\delta)\gamma_{xz} + ka(a+\delta)\gamma_{yz} + (a-\delta)u''' - (a+\delta)v''' - kaw''']^2 \\
&\quad + [(a+\delta)^2\varepsilon_x + (a-\delta)^2\varepsilon_y + k^2a^2\varepsilon_z + (\delta^2-a^2)\gamma_{xy} \\
&\quad + ka(a+\delta)\gamma_{xz} - ka(a-\delta)\gamma_{yz} - (a+\delta)u''' + (a-\delta)v''' - kaw''']^2\} \\
&\quad + \frac{1}{2}k_{\theta}\{[2a(a+\delta)\varepsilon_x + 2a(\delta-a)\varepsilon_y - 2k^2a^2\varepsilon_z + 2a\delta\gamma_{xy} + ka\delta\gamma_{xz} + ka(\delta-2a)\gamma_{yz} + (2a+\delta)u''' + \delta v'''']^2 \\
&\quad + [2a(\delta-a)\varepsilon_x + 2a(a+\delta)\varepsilon_y - 2k^2a^2\varepsilon_z + 2a\delta\gamma_{xy} + ka(\delta-2a)\gamma_{xz} + ka\delta\gamma_{yz} + \delta u''' + (2a+\delta)v''']^2 \\
&\quad + [-2a(a+\delta)\varepsilon_x + 2a(a-\delta)\varepsilon_y - 2k^2a^2\varepsilon_z - 2a\delta\gamma_{xy} + ka(2a+\delta)\gamma_{xz} + ka\delta\gamma_{yz} + \delta u''' + (\delta-2a)v''']^2 \\
&\quad + [2a(a-\delta)\varepsilon_x - 2a(a+\delta)\varepsilon_y - 2k^2a^2\varepsilon_z - 2a\delta\gamma_{xy} + ka\delta\gamma_{xz} + ka(2a+\delta)\gamma_{yz} + (\delta-2a)u''' + \delta v''']^2 \\
&\quad + [2a(a-\delta)\varepsilon_x - 2a(a+\delta)\varepsilon_y - 2k^2a^2\varepsilon_z - 2a\delta\gamma_{xy} - ka\delta\gamma_{xz} - ka(2a+\delta)\gamma_{yz} + (2a-\delta)u''' - \delta v''']^2 \\
&\quad + [-2a(a+\delta)\varepsilon_x + 2a(a-\delta)\varepsilon_y - 2k^2a^2\varepsilon_z - 2a\delta\gamma_{xy} - ka(2a+\delta)\gamma_{xz} - ka\delta\gamma_{yz} - \delta u''' + (2a-\delta)v''']^2 \\
&\quad + [2a(\delta-a)\varepsilon_x + 2a(a+\delta)\varepsilon_y - 2k^2a^2\varepsilon_z + 2a\delta\gamma_{xy} + ka(2a-\delta)\gamma_{xz} - ka\delta\gamma_{yz} - \delta u''' - (2a+\delta)v''']^2
\end{aligned}
$$

$$
\begin{aligned}
&+[2a(a+\delta)\varepsilon_x+2a(\delta-a)\varepsilon_y-2k^2a^2\varepsilon_z+2a\delta\gamma_{xy}-ka\delta\gamma_{xz}+ka(2a-\delta)\gamma_{yz}-(2a+\delta)u'''-\delta v'''']^2\}\\
&+\frac{1}{2}k'_\theta\{8a^2(a\varepsilon_x+a\varepsilon_y-k^2a\varepsilon_z+a\gamma_{xy}-kw''')^2\\
&+4[(\delta^2-a^2)\varepsilon_x+(\delta^2-a^2)\varepsilon_y+k^2a^2\varepsilon_z+(a^2+\delta^2)\gamma_{xy}-ka\delta\gamma_{xz}-ka\delta\gamma_{yz}+\delta u'''+\delta v'''-kaw''']^2\\
&+4[(\delta^2-a^2)\varepsilon_x+(\delta^2-a^2)\varepsilon_y+k^2a^2\varepsilon_z+(a^2+\delta^2)\gamma_{xy}+ka\delta\gamma_{xz}+ka\delta\gamma_{yz}-\delta u'''-\delta v'''-kaw''']^2\}, \qquad (1)
\end{aligned}
$$

where δ is the displacement along both the x and the y directions of the reconstructed surface atoms,[17,30] (k_b, k_θ, k'_θ) are three independent force constants that can be obtained in Ref. [13], and the internal strain components can be expressed as

$$
\begin{aligned}
u''' &= \frac{a^3\delta^2[2k_\mathrm{b}(k'_\theta+2k_\mathrm{b})-k_\theta^2]k\gamma_{xz}+[a^5(k_\theta+2k_\mathrm{b})(k_\theta-2k_\mathrm{b})-a^3\delta^2k_\theta^2k'^2_\theta]k\gamma_{yz}}{a^2[(a^2+\delta^2)(k_\theta+2k_\mathrm{b})+\delta^2k'_\theta](k_\theta+2k_\mathrm{b})},\\
v''' &= \frac{a^3\delta^2[2(k'_\theta+2k_\mathrm{b})-k_\theta^2]k\gamma_{yz}+[a^5(k_\theta+2k_\mathrm{b})(k_\theta-2k_\mathrm{b})-a^3\delta^2k_\theta^2k'^2_\theta]k\gamma_{xz}}{a^2[(a^2+\delta^2)(k_\theta+2k_\mathrm{b})+\delta^2k'_\theta](k_\theta+2k_\mathrm{b})},\\
w''' &= \frac{\delta^2}{2a}(\varepsilon_x+\varepsilon_y)+\left[\frac{\delta^2}{2a}+\frac{a(k'_\theta-2k_\mathrm{b})}{k'_\theta+2k_\mathrm{b}}\gamma_{xy}\right]. \qquad (2)
\end{aligned}
$$

It is worth noting that the strain energy and the internal strain of other types of cells can be obtained in the same way,[13,28] and here we do not give the expressions for succinctness. Then the total strain energy U^tot of the SiNCs can be obtained by the sum of all cells

$$
\begin{aligned}
&U^\mathrm{tot}\\
&=\sum_i\sum_j\sum_l^{2N}U_{ijl}^\mathrm{Bulk}\\
&+\sum_i\sum_j\sum_l^{n}\left(\frac{2n-1}{2}U_{ijl}^\mathrm{SREL}+U_{ijl}^\mathrm{T-SREC-SREL}\right)\\
&+\sum_i\sum_j\sum_l^{n}\left(\frac{2n-1}{2}U_{ijl}^\mathrm{SREL}+U_{ijl}^\mathrm{B-SREC-SREL}\right). \qquad (3)
\end{aligned}
$$

Because of the periodicity of the crystal lattice and the (2×1) SREC in the x–y plane, the periodic calculation element is chosen to contain $4N+4n$ ($=2\times1\times(2N+2n)$) crystal cells. Thus, the calculation element volume is $V^\mathrm{tot}=8a\times4a\times H$, where H is the thickness of the SiNC. Based on the discrete nature (DN) along the thickness direction, it is reasonable to define the nanocantilever thickness as the product of the thickness of one atom layer multiplied by the number of the atom layers,[31] which gives $H=(8N+8nk+k)a$. Consequently, the average strain density of the element can be calculated by $f=U^\mathrm{tot}/V^\mathrm{tot}$. After obtaining the average strain energy density f, according to expression $C_{ij}=\partial^2 f/\partial\varepsilon_{ij}^2$, six independent nonzero elastic constants of the SiNC can be obtained, and then the Young's modulus and the Poisson's ratio of the SiNC in the simple tension state with the SREL and the (2×1) SREC taken into consideration can be respectively derived to be

$$
E_\mathrm{sck}=\frac{(C_{11}-C_{12})(C_{11}C_{33}+C_{12}C_{33}-2C_{13}^2)}{(C_{11}C_{33}-C_{13}^2)(1-v_\mathrm{sck}^2)}, \qquad (4)
$$

$$
v_\mathrm{sck}=(C_{12}C_{33}-C_{13}^2)/(C_{11}C_{33}-C_{13}^2), \qquad (5)
$$

where

$$
\begin{aligned}
C_{11} &= \frac{1}{(8N+8kn+k)a^3}\\
&\times\Bigg((4n-2)a^4(2k_\mathrm{b}+2k_\theta+k'_\theta)\\
&+4Na^4(2k_\mathrm{b}^0+3k_\theta^0)\\
&+k_\mathrm{b}\Bigg\{8(a-\delta)^4+\left[(a+\delta)^2-\frac{\delta^2}{2}\right]^2\\
&+\left[(a-\delta)^2-\frac{\delta^2}{2}\right]^2+2\left(a^2+\frac{\delta^2}{2}\right)^2\Bigg\}\\
&+\frac{k_\theta}{2}\left[4a^2(a+\delta)^2+4a^2(a-\delta)^2\right]\\
&+\frac{k'_\theta}{2}(2a^2-\delta^2)^2\Bigg), \qquad (6)\\
C_{12} &= \frac{1}{(8N+8kn+k)a^3}\\
&\times\Bigg((4n-2)a^4(2k_\mathrm{b}-2k_\theta+k'_\theta)\\
&+4Na^4(2k_\mathrm{b}^0-k_\theta^0)\\
&+k_\mathrm{b}\Bigg\{8(a-\delta)^4+2\left[(a+\delta)^2-\frac{\delta^2}{2}\right]\\
&\times\left[(a-\delta)^2-\frac{\delta^2}{2}\right]+2\left(a^2+\frac{\delta^2}{2}\right)^2\Bigg\}\\
&+4k_\theta a^2\left(\delta^2-a^2\right)+\frac{k'_\theta}{2}\left(2a^2-\delta^2\right)^2\Bigg), \qquad (7)
\end{aligned}
$$

$$C_{13} = \frac{1}{(8N+8kn+k)a^3}[4na^4(2k^2k_{\rm b} - k^2k'_{\theta}) + 4Na^4(2k_{\rm b}^0 - k_{\theta}^0) + 2k_{\rm b}k^2a^2\delta^2 + k'_{\theta}k^2a^2\delta^2], \quad (8)$$

$$C_{33} = \frac{1}{(8N+8kn+k)a^3}[4na^4(2k^4k_{\rm b} + 2k^4k_{\theta} + k^4k'_{\theta}) + 4Na^4(2k_{\rm b}^0 + 3k_{\theta}^0)], \quad (9)$$

and $k_{\rm b}^0$ and k_{θ}^0 are the equilibrium force constants of the unrelaxed silicon crystal cell.

2.2. SCK model for resonant frequency of the bending SiNC with large deformation

It is well known that experimental methods can be used to measure the deflections or the resonant frequencies of bending nanostructures to acquire elastic and resonant properties. Hence, in addition to the SREC and the SREL, the adsorption-induced SSTR also plays an important role in the size-dependent mechanical properties of nanostructures. Consider an Euler–Bernoulli SiNC with adsorption-induced SSTR, as shown in Fig. 1(a), when the lateral load at initial time ($t = 0$) is imposed, the initial instantaneous displacement of the static bending SiNC reaches the maximum, and the maximum mechanical strain potential energy $U_{\max}$ within the framework of nonlinear finite deformation kinematics can be written as

$$U_{\max} = \frac{E_{\rm sck}B}{2}\int_0^A \int_{-\frac{H}{2}}^{\frac{H}{2}} \left[-z\frac{{\rm d}^2w(x)}{{\rm d}x^2} + \frac{1}{2A}\int_0^A \left(\frac{{\rm d}w(x)}{{\rm d}x}\right)^2 {\rm d}x\right]^2 {\rm d}z{\rm d}x + \frac{\gamma\Omega}{2}\left[1 - v_{\rm sck} - \frac{v_{\rm sck}}{2A}\int_0^A \left(\frac{{\rm d}w(x)}{{\rm d}x}\right)^2 {\rm d}x\right] \times \int_0^A \left(\frac{{\rm d}w(x)}{{\rm d}x}\right)^2 {\rm d}x, \quad (10)$$

where the first term is the sum of the bending strain potential energy and the stretching strain potential energy, the second term is the strain potential energy induced by the strain-dependent adsorption-induced SSTR, $E_{\rm sck}$ is the Young's modulus of the SiNC in the simple tension state with the SREL and the SREC taken into consideration and is given by Eq. (4), $v_{\rm sck}$ is the Poisson's ratio given by Eq. (5), A and B are the length and the width of the SiNC ($A \geq B \geq 5H$), respectively, Ω is the contour length of the cross section, γ is the adsorption-induced SSTR, which is assumed to exist on all surfaces of the SiNC in the current model, the typical adsorption-induced SSTR reported in Ref. [25] is about 0.5 mN/m, $w(x)$ is the deflection, and an assumed deflection shape function in the form of a cosine satisfying the boundary conditions is selected[32]

$$w(x) = 2w_0\sin^2\left(\frac{\pi x}{4A}\right) = w_0\left(1 - \cos\frac{\pi x}{2A}\right), \quad (0 \leq x \leq A) \quad (11)$$

with w_0 being the maximum deflection (vibration amplitude) of the SiNC, whose value is usually in the order of a few tenths to several tens nanometers.[18,33,34]

Substituting Eq. (11) into Eq. (10), we obtain the maximum mechanical strain potential energy $U_{\max}$ as

$$U_{\max} = \frac{\pi^4(BHE_{\rm sck} - 2\gamma\Omega v_{\rm sck})}{512A^3}w_0^4 + \frac{\pi^4BH^3E_{\rm sck} + 48\pi^2\gamma\Omega A^2(1 - v_{\rm sck})}{768A^3}w_0^2. \quad (12)$$

When the external load is removed, the SiNC freely vibrates with frequency ω and mode shape $w(x)$, and its instantaneous deflection shape function can be expressed as

$$w(x,t) = w(x)\cos\omega t. \quad (13)$$

Obviously, the equilibrium position of the SiNC corresponds to the plane state without bending, and when it passes through the equilibrium position, we have $w = 0$, and the speed reaches the maximum, i.e., $\pm\omega w(x)$. At this time, the elastic strain potential energy of the SiNC is zero, whereas the kinetic energy reaches the maximum, and the maximum kinetic energy is

$$K_{\max} = \frac{1}{2}\bar{m}\int_0^A \left(\frac{\partial w(x,t)}{\partial t}\right)^2 {\rm d}x = \frac{1}{2}\bar{m}\omega^2\int_0^A w^2(x){\rm d}x = \left(\frac{3}{4} - \frac{2}{\pi}\right)\rho BHAw_0^2\omega^2, \quad (14)$$

where $\bar{m}$ is the mass per unit length of the SiNC, and ρ is the mass density of silicon.

According to energy conversion and conservation, the mechanical strain potential energy of the SiNC furthest away from the equilibrium position should be equal to its kinetic energy at the equilibrium position[35,36]

$$U_{\max} = K_{\max}. \quad (15)$$

Substituting Eqs. (12) and (14) into Eq. (15) gives the analytical solution to the nonlinear fundamental resonant frequency of the SiNC with surface effects

$$f_{\rm sck} = \frac{\omega}{2\pi} = \left(1 + \frac{4\gamma\Omega A^2(1-v_{\rm sck})}{E_{\rm sck}I\pi^2} + \frac{E_{\rm sck}BH - 2\gamma\Omega\nu_{\rm sck}}{8E_{\rm sck}I}w_0^2\right)^{1/2} \times \frac{\lambda^2}{2A^2}\sqrt{\frac{E_{\rm sck}I}{\rho BH}}\,, \quad (16)$$

where $\lambda \approx 1.058$ is a mode shape factor that takes into account the error caused by the assumed deflection shape function, and $I = BH^3/12$ is the moment of inertia. It is worth noting that if the finite deformation kinematics (nonlinear large deformation) and the surface effects in Eq. (16) are neglected, $w_0 \to 0$, $\gamma \to 0$, $E_{\rm sck} \to E_{\rm bulk}$, Eq. (16) is the same as the following equation obtained in the classical linear beam theory:[22]

$$f_{\rm bulk} = \frac{\eta^2}{2\pi A^2}\sqrt{\frac{E_{\rm bulk}I}{\rho BH}}\,, \quad (17)$$

where $\eta = 1.875$ is for the fundamental resonant mode.

3. Results and discussion

We first investigate the influences of the surface effects on the size-dependent elastic properties of the SiNCs. It can be seen from Eqs. (4)–(9) that the Young's modulus of the SiNC in the simple tension state is a function of thickness H (including the DN), the displacement of the reconstructed surface atoms δ, and the SREL coefficient k. Evidently, this supports the idea that their values may determine the size effects of the Young's modulus and the Poisson's ratios. In order to determine the relative contributions of the DN along the thickness direction, the SREC, and the SREL on the overall elastic response of the SiNC, as shown in Fig. 2, we calculate the normalized Young's modulus and the normalized Poisson's ratios of the ultrathin SiNCs that have the thicknesses ranging from 1.5 nm to 25 nm, which will be prevalent in the NEMS design. The values of the parameters in our calculations are listed in Table 1.

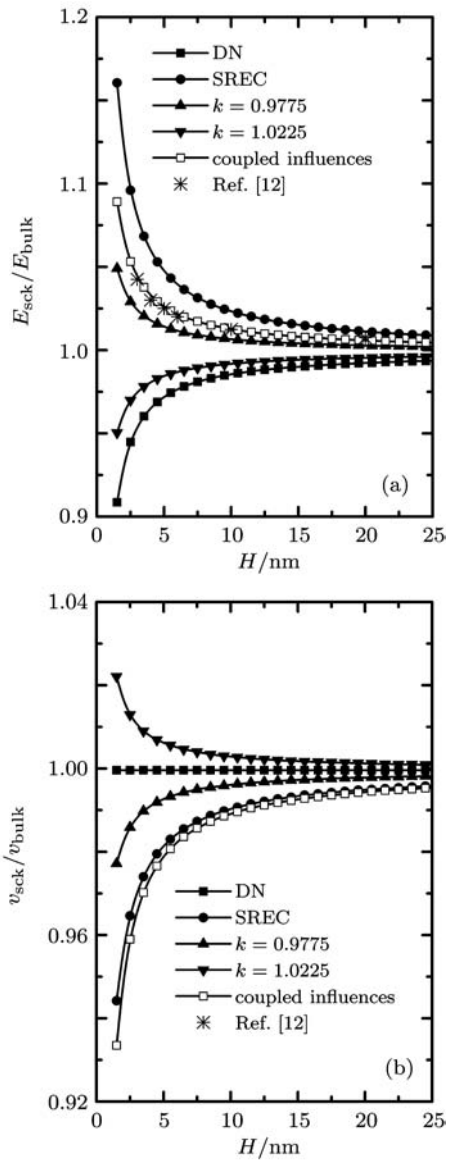


Fig. 2. (a) Normalized Young's modulus and (b) normalized Poisson's ratios of the SiNCs each as a function of thickness.

On one hand, as can be observed from Fig. 2(a), the SCK model indicates that the normalized Young's modulus of the SiNC is size-dependent for the case without the SREC and the SREL, and it obviously decreases as the thickness decreases due to the DN along the thickness direction.[13,17,31] In contract, the SREC results in a significant increase of the bulk Young's modulus as the thickness decreases. The stiffening effects are primarily resulted from the bond saturation and the bond contraction.[12,17] The SCK model also indicates that the influence of a slight SREL on the

Table 1. Parameters used in the calculations.

n	B/nm	ρ/kg·m^{-3}	$k_{\rm b}^0$/N·m^{-3}	k_θ^0/N·m^{-3}	$E_{\rm bulk}$/GPa	δ/Å	k	γ/mN·m^{-1}
1	125	2.33×10^3	6.577×10^{20}	3.743×10^{20}	141	0.5197	0.9925 or 1±0.0225	±0.5

Young's modulus of the SiNC is relatively small. The SREL makes the SiNC slightly stiffer when the surface is contractive ($k = 0.9775$), and slightly softer when the surface is expansive ($k = 1.0225$). The stiffening effects have been attributed to the bond contraction, whereas the softening effects are primarily resulted from the bond expansion. It is noted that all effects mentioned above are coupled together to affect the Young's modulus of the SiNC. In order to validate our current model, we use it to calculate the normalized Young's modulus of the SiNC with the coupled influences of the DN, the SREC, and the SREL ($k = 0.9925$). As can be seen from Fig. 2(a), it is quantitatively consistent with the molecular dynamics results of Ref. [12]. On the other hand, the almost opposite trend is observed in the Poisson's ratios of the SiNCs, as shown in Fig. 2(b). The DN has no contribution to the size effect of the Poisson's ratio of the SiNC. Additionally, both the Young's modulus and the Poisson's ratios of the SiNCs approximately approach the bulk values as the thickness becomes larger than 25 nm, which indicates that the coupled influences of the DN, the SREC and the SREL on the overall elastic response of the large-size SiNC are not expected to be significant and can be neglected.

We next discuss the results for the influences of the surface effects on the linear fundamental bending resonant frequencies of the long and ultrathin SiNCs shown in Fig. 3. In all cases, length A ranges from 750 nm to 1500 nm, thickness H ranges from 1.5 nm to 25 nm, width B is a constant equaling to 125 nm, and the maximum deflection $w_0 \to 0$. In order to ascertain the dominant effect and quantify how the surface effects affect the fundamental resonant frequencies calculated by the SCK model, they are normalized by the corresponding bulk values obtained by using Eq. (17), which is based on the classical linear beam theory. In other words, in these figures, the normalized resonant frequency $f_{\rm sck}/f_{\rm bulk}$ is defined as the ratio of the linear fundamental resonant frequency with the DN or the surface effects to that without the DN and the surface effects.

Figure 3(a) depicts the variations of the normalized linear fundamental resonant frequencies with different lengths and thicknesses due to the DN in the thickness direction or the SREC. As can be observed, the dimensionless normalized resonant frequency is independent of the length but is related to the thickness, and the influence of the DN or the SREC becomes more and more significant as the thickness decreases. This occurs because as the SiNC thickness decreases, the surface area to volume ratio increases. In particular, the DN results in a distinctly decrease in the dimensionless resonant frequency as the thickness decreases, whereas the SREC results in a distinctly increase especially when the thickness is of the order of 5 nm or less. According to Eqs. (16) and (17), we find $f_{\rm sck}/f_{\rm bulk} = (E_{\rm sck}/E_{\rm bulk})^{1/2}$ at this time, so the above results can be expected from the fact that the bulk normalized Young's modulus of the SiNC shows a distinctly decrease (increase) with the decrease of

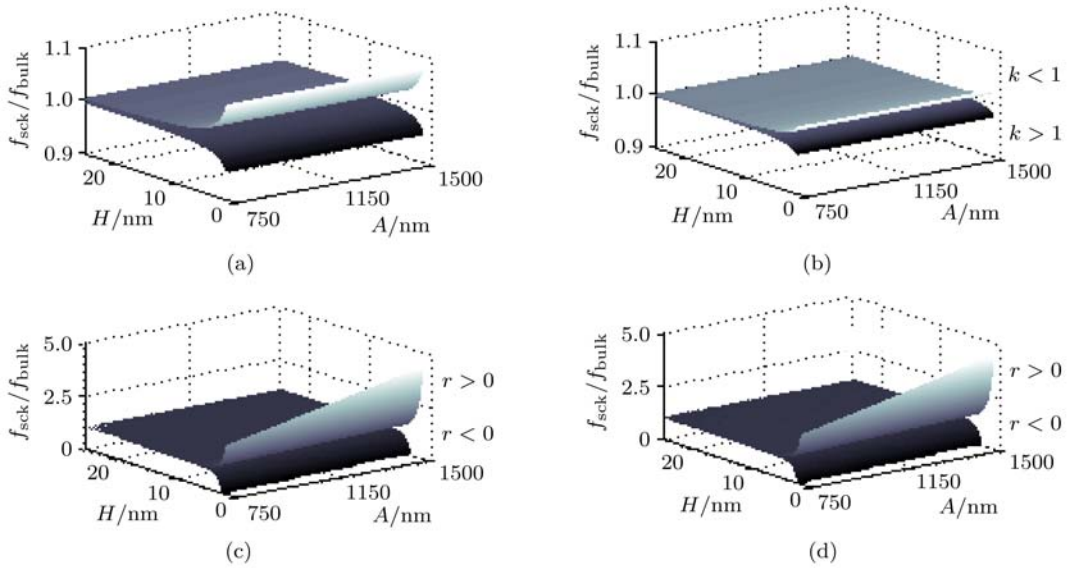


Fig. 3. (color online) Variations of normalized linear fundamental resonant frequencies of the SiNCs with different lengths and thicknesses. (a) The DN or the SREC is considered, (b) a slight SREL ($k = 1\pm0.0225$) is considered, (c) the adsorption-induced SSTR ($\gamma = \pm0.5$ mN/m) is considered, (d) the coupled influences are considered.

the thickness due to the DN (the SREC), and it is independent of the length. Similarly, as shown in Fig. 3(b), the influence of the SREL on the dimensionless normalized resonant frequency of the SiNC is also independent of the length but is related to the thickness. As expected, the SREL makes the dimensionless resonant frequency increase slightly when the surface is contractive ($k = 0.9775$), and decrease slightly when the surface is expansive ($k = 1.0225$).

The variations of the fundamental resonant frequencies due to the adsorption-induced SSTR are plotted in Fig. 3(c). Clearly, the influence of the adsorption-induced STTR on the resonant frequency of the SiNC also depends on the size. For example, when the thickness is larger than 10 nm, $f_{\rm sck}/f_{\rm bulk}$ is close to 1. However, there is a dramatic variation in the ratio as the SiNC thickness decreases and the length increases. When the negative STTR is accounted for, the normalized fundamental resonant frequency significantly drops, whereas the trend is opposite for the case in which parameter γ is of positive sign. As can be seen from Fig. 3(c), when H=1.5 nm, $f_{\rm sck}/f_{\rm bulk}$ is larger than 2, which means that the resonant frequency predicted by the SCK model deviates dramatically from that predicted by the classical continuum model ignoring the SSTR. This occurs because the adsorption-induced SSTR becomes important, which is attributed to the increase of both the surface area to volume ratio and the surface area. Figure 3(d) illustrates the normalized resonant frequencies $f_{\rm sck}/f_{\rm bulk}$ with the coupled influences of the DN, the SREC, and the SREL ($k = 0.9925$) versus different lengths and thicknesses. By comparing Fig. 3(c) with Fig. 3(d), we find a similar behavior, which clearly demonstrates that the adsorption-induced STTR has the largest influence on the fundamental resonant frequencies of the SiNCs.

In all of the above calculations, we consider the linear case of small deformation ($w_0 \to 0$). For practical purposes, we now quantify how the large deformation or the large deflection (vibration amplitude) impacts the fundamental resonant frequencies of the SiNCs. To do so, the effects of the maximum dimensionless vibration amplitude w_0/H on the normalized fundamental resonant frequency ratio $f_{\rm sck}/f_{\rm bulk}$ are plotted in Figs. 4(a) and 4(b) with different thicknesses and different lengths, respectively. From these

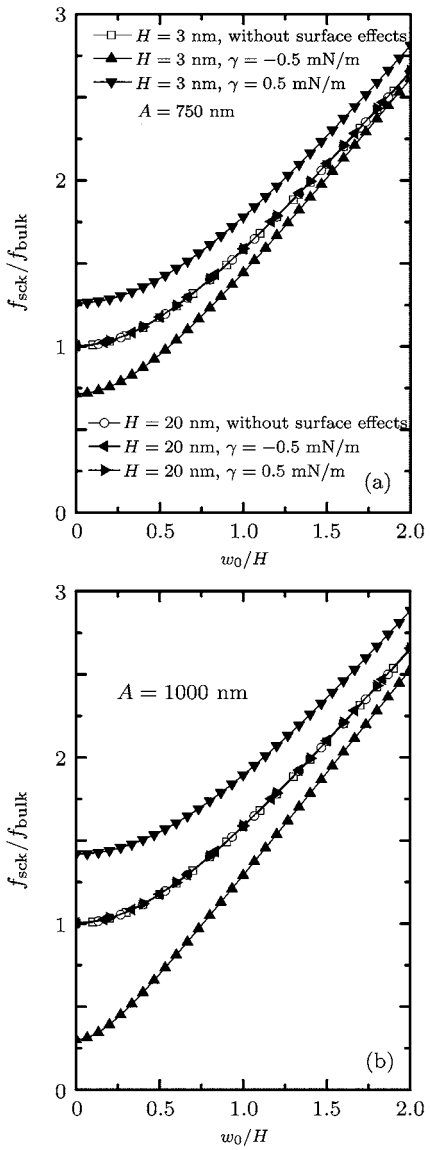


Fig. 4. Variations of normalized nonlinear fundamental resonant frequencies of the SiNCs with aspect ratio w_0/H for (a) A=750 nm and (b) A=1000 nm. Parameters used in the calculation are list in Table 1, the surface effects and the DN are considered.

figures, it is evident that the nonlinear fundamental frequencies increase with the increase of the maximum dimensionless vibration amplitude w_0/H. Moreover, the increasing varying trend depends not only on the thickness of the SiNC but also on its length. It is clear from Figs. 4(a) and 4(b), a larger length in the thinner SiNC results in a larger frequency shift. As mentioned above, this result is mainly attributed to the increasing influences of the surface effects, especially the adsorption-induced SSTR.

However, as shown in Fig. 4, the influences of the surface effects will be less significant for vibrating when the maximum vibration amplitude w_0 increases to several times the thickness H or more. It is also noted that in spite of the different values

of the adsorption-induced SSTR, the nonlinear amplitude frequency response curves of the SiNCs with 20 nm thickness coincide with those without the surface effects, which indicates that the surface effects have no pronounced effect on the nonlinear amplitude frequency response curves of the SiNCs when $H > 20$ nm. In this case, the surface effects can be completely neglected, which is adverse for the design of sensors based on the changes of the frequency shifts, such as chemical and biological sensors. In order to take full advantage of the surface effects, from the results of our calculations, we find the following few points worth being recommended. (i) Let the length of the SiNC as long as possible. ii) Let the thickness of the SiNC as thin as possible. iii) Let the vibration amplitude of the SiNC as small as possible, in other words, a small deformation may be more appropriate for the design of chemical and biological resonant sensors.

4. Comparison with experiment and the other model

In order to validate the SCK model, we attempt to compare the variations of the resonant frequencies of the SiNCs due to surface effects with the available experimental data. However, we find that a direct quantitative comparison cannot be made due to the fact that the SiNCs in the present work are axially aligned in the $\langle 100 \rangle$ direction, whereas the SiNCs in the avaibalbe experiments[2,11] are of the $\langle 110 \rangle$ or the $\langle 111 \rangle$ orientation. Most importantly, the dominant surface effect in current model, i.e., the adsorption-induced STTR, has not been investigated in those experiments. Note that the SCK model is a multi-scale model, which means that it can be used not only to calculate the fundamental resonant frequency of the SiNC, but also to calculate that of the silicon micron cantilever (SiMC). At the same time, considering the adsorption-induced STTR is the most important surface effect, we use the SCK model to determine the fundamental resonant frequencies of the SiMCs with and without the adsorption-induced STTR and quantitatively compare in Table 2 the results with the reported experimental data given in Ref. [25]. The length ($A = 499$ μm), the width ($B = 97$ μm), and the equivalent thickness ($H_{\rm eff}$ is approximately 827 nm with the influences of the titanium and the gold on the top surface of the SiMC and the measurement error considered) are based on the values from Ref. [25]. From Table 2, we find that our present results based on the SCK model agree well with the experimental data. In particular, a less than 0.5% variation between the resonant frequencies predicted in our SCK model and the experimental measured resonant frequencies is shown in Table 2. This result demonstrates that the multi-scale SCK model is reliable and can be used to predict and analyze the resonant properties (before and after adsorption) of silicon cantilevers.

Table 2. Measured resonant frequencies before (f^0) and after (f^γ) adsorption and the corresponding calculated values ($f^0_{\rm sck}$ and $f^\gamma_{\rm sck}$) using the SCK model. All frequencies are in the unit of Hz.

$H_{\rm eff}$/nm	f^0	$f^0_{\rm sck}$	f^γ	$f^\gamma_{\rm sck}$
822	4550	4556	4590	4577
823	4560	4562	4570	4567
834	4620	4622	4640	4633

We also note that based on the continuum beam theory, an empirical formula was proposed for the fundamental resonant frequency of the silicon cantilever with the adsorption-induced SSTR in Ref. [25], which is given as

$$f^\gamma_{\rm bulk} = \left(1 + \frac{2\gamma A^3}{E_{\rm bulk} I \pi^2}\right)^{1/2} \frac{\eta^2}{2\pi A^2} \sqrt{\frac{E_{\rm bulk} I}{\rho B H}} \,. \quad (18)$$

The bracketed term in Eq. (18) shows the influence of the adsorption-induced SSTR. The compressive or the tensile SSTR (i.e., $\gamma < 0$ or $\gamma > 0$) will decrease or increase the resonant frequencies, which is qualitatively consistent with our above results based on the SCK model, i.e., Eq. (16). In order to quantitatively compare the fundamental resonant frequencies predicted by the current model and by Eq. (18), the dimensionless linear free vibration frequency shifts $\Delta f / f^\gamma_{\rm bulk}$ of the SiNCs with different aspect ratios A/H are plotted in Fig. 5, where $\Delta f = f_{\rm sck} - f^\gamma_{\rm bulk}$ is the shift of the fundamental resonant frequency.

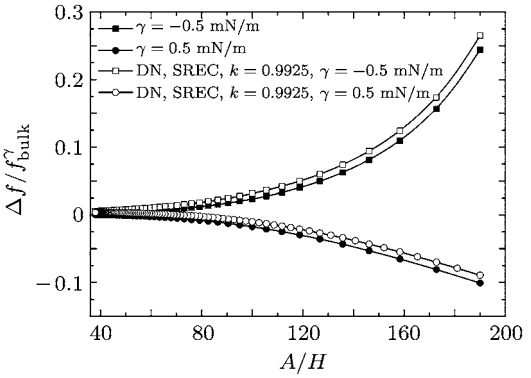


Fig. 5. Resonant frequency shifts of the SiNCs as functions of aspect ratio A/H.

From Fig. 5, it can be found that $\Delta f/f^{\gamma}_{\rm bulk} \to 0$ due to the slight influence of the SSTR when the length-to-thickness ratio $A/H < 60$, which means that in this case the SCK model and the empirical formula (Eq. (18)) give similar results in quantitatively predicting the adsorption-induced SSTR induced resonance shift. However, as the length-to-thickness ratio further increases, a more and more obvious discrepancy between our SCK model and Eq. (18) can be observed in Fig. 5, which indicates that the length-to-thickness ratio is the key parameter correlating the deviations in the resonant frequencies predicted from the current model and the empirical formula. For example, when $A/H = 190$, the resonant frequency of the SiNC with the tensile SSTR calculated by the SCK model decreases to nearly 10% lower than the corresponding value calculated by Eq. (18). In contrary, when the compressive SSTR is accounted for, a nearly 25% increase for the SCK model is demonstrated in Fig. 5. The above results show that the adsorption-induced SSTR has a more significant effect on the resonant properties of the SiNCs based on Eq. (18) than that predicted by the SCK model. This occurs mainly because of the fact that the degree of influence of the length-to-thickness ratio A/H is different in the two models. Equation (18) indicates that the effect of the SSTR is proportional to factor $(A/H)^3$. While, in the SCK model, the effect of the SSTR is approximately proportional to factor $(A/H)^2$. Obviously, the impact of cubic term $(A/H)^3$ is greater than that of square term $(A/H)^2$. Thus, the above results can be directly explained by the difference of the two factors. And moreover, as the aspect ratio A/H increase, the influence of the SSTR on the resonant frequency of the SiNC through factor $(A/H)^3$ or $(A/H)^2$ becomes extremely sensitive to the difference of the two factors. In this case ($A/H > 60$), compared to our current SCK model, the empirical formula (Eq. (18)) may overestimate the influence of the SSTR on the resonant frequency of the SiNC. Besides, it is noted that the empirical formula is originally proposed for the fundamental resonant frequency of the SiMC, thus it has not considered the coupled influence of the DN, the SREC, and the SREL. However, the SCK model can easily consider this coupled influence. As shown in Fig. 5, the curve with the coupled influence deviates from that without the coupled influence. In particular, the DN, the SREC, and the SREL have significant coupled effect for such a SiNC with a large length-to-thickness ratio, which means neglecting either of these in the SCK model will result in errors for the prediction of the resonant behavior of the SiNC.

5. Conclusion

In summary, based on energy conversion and conservation, a large-deflection semi-continuum atomistic lattice Keating model has been proposed to study the elastic and the resonant properties of long and ultra-thin SiNCs. The analytical solutions for the Young's modulus and the Poisson's ratio of the SiNC in the simple tension state and the fundamental resonant frequency of the SiNC in bending can be obtained respectively. It is found that the fundamental resonant frequency has additional terms associated with the maximum deflection and the surface effects compared to the conventional solutions without the surface effects. The calculated results clearly show the size-and surface-dependent elastic responses of the SiNCs, which are consistent with the previous atomistic study. The SCK model also indicates that the adsorption-induced SSTR has the most important effect on the resonant frequency shift of the SiNC, followed by the DN and the SREC, whereas the SREL has the least effect. And moreover, we find that the large deformation increases the nonlinear fundamental frequency of the SiNC, depending not only on its size but also on the surface effects. Additionally, it is noticed that the predictions of the resonant frequency shifts due to the adsorption-induced surface stress from the current model agree well with the experimental data, and the length-to-thickness ratio is the key parameter that correlates the deviations in the resonant frequencies predicted by the SCK model and the other existing model. This work might be helpful for characterizing the resonant properties of the SiNCs and the design of nanocantilever-based resonators and sensors in the NEMS.

References

[1] Craighead H G 2000 *Science* **290** 1532

[2] Li X X, Ono T, Wang Y L and Esashi M 2003 *Appl. Phys. Lett.* **83** 3081

[3] Kizuka T, Takatani Y, Asaka K and Yoshizaki R 2005 *Phys. Rev.* B **72** 035333

[4] Cui Y, Zhong Z H, Wang D L, Wang W U and Lieber C M 2003 *Nano Lett.* **3** 149

[5] Li D, Wu Y, Kim P, Shi L, Yang P and Majumdar A 2003 *Appl. Phys. Lett.* **83** 2934

[6] Wu Z Y, Liu K X and Ren X T 2010 *Chin. Phys.* B **19** 097806

[7] Zhang J H, Huang Q A, Yu H and Lei S Y 2008 *Chin. Phys.* B **17** 4292
[8] Yang Y L and Li X X 2011 *Nanotechnology* **22** 015501
[9] Soon B W, Neuzil P, Wong C C, Reboud J, Feng H H and Lee C K 2010 *Procedia Engineering* **5** 1127
[10] Agarwal A, Buddharaju K, Lao I K, Singh N, Balasubramanian N and Kwong D L 2008 *Sensor. Actuat.* A **145**–**146** 207
[11] Feng X L, He R R, Yang P D and Roukes M L 2007 *Nano Lett.* **7** 1953
[12] Shim H W, Zhou L G, Huang H C and Cale T S 2005 *Appl. Phys. Lett.* **86** 151912
[13] Zhang J H, Huang Q A, Yu H and Wang J 2009 *J. Phys.* D: *Appl. Phys.* **42** 045409
[14] Guo J G and Zhao Y P 2007 *Nanotechnology* **18** 295701
[15] Dingreville R, Qu J M and Cherkaoui M 2005 *J. Mech. Phys. Solids* **53** 1827
[16] Miller R E and Shenoy V B 2000 *Nanotechnology* **11** 139
[17] Wang J, Huang Q A and Yu H 2008 *Chin. Phys. Lett.* **25** 1403
[18] Fu Y M, Zhang J and Jiang Y J 2010 *Physica* E **42** 2268
[19] Liang L H, Ma H S and Wei Y G 2011 *J. Nanomater.* **2011** 670857
[20] Sadeghian H, Goosen J F L, Bossche A, Thijsse B J and van Keulen F 2010 *Thin Solid Films* **518** 3273
[21] Lee B and Rudd R E 2007 *Phys. Rev.* B **75** 195328
[22] Park H S 2008 *J. Appl. Phys.* **103** 123504
[23] Park H S 2009 *Nanotechnology* **20** 115701
[24] Feng Y K, Liu Y L and Wang B 2011 *Acta Mech.* **217** 149
[25] McFarland A W, Poggi M A, Doyle M J, Bottomley L A and Colton J S 2005 *Appl. Phys. Lett.* **87** 053505
[26] Zhang J H, Gu F, Liu Q Q, Gu B and Li M 2010 *Acta Phys. Sin.* **59** 4226 (in Chinese)
[27] Jia Z M, Yang G Q, Cheng Z N, Liu X H and Zou S C 1994 *Acta Phys. Sin.* **43** 609 (in Chinese)
[28] Keating P N 1966 *Phys. Rev.* **145** 637
[29] Rücker H and Methfessel M 1995 *Phys. Rev.* B **52** 11059
[30] Batra I P 1990 *Phys. Rev.* B **41** 5048
[31] Sun C T and Zhang H 2003 *J. Appl. Phys.* **93** 1212
[32] Huang D W 2008 *Int. J. Solids Struct.* **45** 568
[33] Carr D W, Evoy S, Sekaric L, Craighead H G and Parpia J M 1999 *Appl. Phys. Lett.* **75** 920
[34] San Paulo A, Black J P, White R M and Bokor J 2007*Appl. Phys. Lett.* **91** 053116
[35] Cao G B, Chen Y F, Jiao J W and Wang Y L 2007 *Mech. Res. Commun.* **34** 503
[36] Gu F, Zhang J H, Yang L J and Gu B 2011 *Acta Phys. Sin.* **60** 056103 (in Chinese)